Published in final edited form as:
Biochem Biophys Res Commun. 2009 July 24; 385(2): 181–186. doi:10.1016/j.bbrc.2009.05.035.

Lipid Nanopores Can Form a Stable, Ion Channel-Like Conduction Pathway in Cell Membrane

Andrei G. Pakhomov[a,*], **Angela M. Bowman**[a], **Bennett L. Ibey**[b], **Franck M. Andre**[a], **Olga N. Pakhomova**[a], and **Karl H. Schoenbach**[a]

[a]Frank Reidy Research Centre for Bioelectrics, Old Dominion University, Norfolk, VA

[b]Radio Frequency Radiation Branch, Human Effectiveness Directorate, Air Force Research Laboratory, Brooks City Base, San Antonio, TX

Abstract

Cell permeabilization by electric pulses (EPs), or electroporation, has been well established as a tool to indiscriminately increase membrane flows of water solutes down the concentration and voltage gradients. However, we found that EPs of nanosecond duration (nsEPs) trigger formation of voltage-sensitive and inward-rectifying membrane pores. NsEP-treated cells remain mostly impermeable to propidium, suggesting that the maximum pore size is ~1 nm. The ion-channel- like properties of nsEP-opened nanopores vanish if they break into larger, propidium-permeable "conventional" pores. However, nanopores can be stable for many minutes and significantly impact cell electrolyte and water balance. Multiple nsEPs cause fast cell swelling and blebbing, whereas opening of larger pores with digitonin abolishes swelling and causes blebs to implode. The lipid nature of nsEP-opened nanopores is confirmed by fast externalization of phosphatidylserine residues. Nanopores constitute a previously unexplored ion transport pathway that supplements classic ion channels but is distinctly different from them.

Keywords

electroporation; membrane lipids; electric pulses; membrane permeability; pores

Introduction

The phenomenon of dielectric breakdown of cell membrane by high-voltage electric pulses, or electroporation, has been known for several decades. Although the mechanism of electroporation has not been fully understood, this technique found many applications in intracellular delivery of drugs, dyes, and plasmids, in cancer therapy and immune stimulation [1–4]. In contrast to the conventional electroporation, nsEPs produce bioeffects without triggering an uptake of membrane integrity marker dyes, such as propidium^{+} and Trypan blue [5–9]. This phenomenon is interpreted as a direct intracellular effect of the electric field, or implies that the pores opened by nsEPs are too small for dye molecules. The latter point of

*Corresponding author: Andrei G. Pakhomov, Frank Reidy Research Center for Bioelectrics, 830 Southampton Avenue, Suite 5100, Old Dominion University, Norfolk, VA 23510, USA, (210) 2049012, (757) 3142397 (fax), andrei@pakhomov.net.

view was corroborated by: (a) analytical and molecular dynamics modeling of membrane effects of nsEP [10,11], (b) demonstration of phosphatidylserine (PS) externalization from the internal membrane face [9,12], and (c) direct measurements of membrane electrical conductance [5,13]. Box dimensions of the propidium cation calculated from its crystal structure are 13.8 × 11.5 × 5.4 A, so the upper limit for the diameter of nsEP-opened electropores can be estimated at about 1–1.5 nm. Most importantly, the recovery of membrane conductance due to pore resealing took as long as several minutes [13], hence the technique of lipid nanopore activation by nsEP presented a unique opportunity to explore nanopore properties in live cells by conventional electrophysiology and confocal microscopy methods.

Below we demonstrate that nanopores are qualitatively different from plain “holes” in the lipid bilayer and exert complex behaviors that are traditionally expected only from sophisticated molecular devices like protein ion channels. We also provide a discussion of mechanisms that make these behaviors possible and of nanopores’ potential role in transmembrane water and electrolyte balance.

Materials and Methods

Propagation of cells

GH3 (a murine pituitary) and CHO-K1 (Chinese hamster ovary) cell lines were obtained from ATCC (Manassas, VA) and grown in 75-cm^2 flasks at 37°C with 5% CO_2 in air. GH3 cells were cultured in Ham’s F12K medium supplemented with 2.5% fetal bovine serum (FBS) and 15% horse serum. CHO cells were propagated in Ham’s F12K medium supplemented with 10% FBS. The growth media also contained 1% penicillin/streptomycin. For the passage immediately preceding the experiments, cells were transferred onto glass cover slips pre-treated with poly-L-lysine.

Electrophysiology and cell imaging

Patch pipettes were pulled from a borosilicate glass (BF150-86-10, Sutter, Novato, CA) to a tip diameter of 1–2 μm on a Flaming/Brown P-97 puller (Sutter). A cover slip with cells was placed into a glass-bottomed chamber (Warner Instruments, Hamden, CT) mounted on an Olympus IX71 inverted microscope equipped with an FV 300 confocal laser scanning system (Olympus America, Center Valley, PA). Cell images were obtained with a 40x,0.75 NA, no-immersion objective (the same as was used for pipette guidance in electrophysiology measurements). Whole-cell and outside-out incised patch currents were recorded in a voltage-clamp mode using a Multiclamp 700B amplifier, Digidata 1322A A–D converter, and pCLAMP10 software (MDS, Foster City, CA). The data were corrected for junction potential when applicable. All experiments were performed at room temperature of 22–24 °C.

For experiments illustrated in Fig. 1**a**, the bath and pipette buffers contained, respectively (hereinafter in mM): 135 NaCl, 5 KCl, 2 $MgCl_2$, 10 HEPES (pH 7.4), and: 150 KCl, 1 NaCl, 2 $MgCl_2$, 5 HEPES (pH 7.2). The same bath buffer supplemented with 30 μg/ml of propidium iodide (PI) was used to record morphological changes in cells (Fig. 5,**c**). For symmetrical solution conditions (Fig. 1**b**), both the bath and pipette contained 140 K-Acetate, 5 K-EGTA, 4 $MgCl_2$, and 10 HEPES (pH 7.2); in other experiments (Fig. 1**c** and Fig 2), K^+ was replaced with Cs^+, and (Fig. 2) 30 μg/ml of PI was added to the bath buffer only. The osmolarity of all solutions was between 290 and 310 mOsm as measured with a freezing point microosmometer (Advanced Instruments, Inc., Norwood, MA, USA). Chemicals were purchased from Sigma-Aldrich (St. Louis, MO).

Real-time imaging of Tl^+ uptake by cells was accomplished using a FluxOR™ Thallium Detection Kit (Invitrogen, Eugene, OR). Cells were loaded with a Tl^+-sensitive fluorophore

as per manufacturer's instructions. For nsEP exposure, cells were transferred into a bath buffer containing 8 Tl_2SO_4, 70 Cs-Acetate, 2 $MgSO_4$, 2 Ca-Acetate, 50 TEA-Acetate, 5 4-aminopyridine, 10 HEPES, and 10 glucose (pH 7.4); in some experiments, the buffer also contained 30 μg/ml of PI. The same buffer but without Tl_2SO_4 (replaced with an isoosmotic amount of Cs-Acetate) was used for negative control measurements and as a holding bath buffer when perfusion with Tl^+ was delayed (Fig. 3b).

Externalization of PS was visualized by adding Annexin V-FITC solution (BD Biosciences, Franklin Lakes, NJ) at 10x dilution to a bath buffer containing 135 NaCl, 5 KCl, 2 $CaCl_2$, 2 $MgCl_2$, 10 HEPES, 10 glucose, and 40 μg/ml of PI (pH 7.4).

The dyes were excited with a blue laser (488 nm). Emission was recorded at 605 nm for propidium and at 530 nm for Annexin V-FITC and Tl^+ fluorescence signals. Photomultiplier tube settings for 605 nm emission were biased towards maximum sensitivity and detection of even minimal propidium uptake if it takes place. Images were quantified with MetaMorph v. 7.5 (MDS).

Nanosecond pulse stimulation and local E-field modeling

Nearly rectangular 600-ns pulses were generated in a transmission line-type circuit, by closing a MOSFET switch upon delivery of a TTL trigger pulse from pClamp software via a Digidata output. NsEP were delivered to a selected cell with a pair of tungsten rod electrodes (0.1-mm diameter, 0.16-mm gap). The position of pulser electrodes relative to the selected cell and patch-clamp recording pipette is illustrated in Fig. 1 (inset). The exact pulse shapes and amplitudes were captured and measured with a 5-GHz TDS 3052 oscilloscope (Tektronix, Beaverton, OR). The E-field at the cell location between the electrodes was determined by 3D simulations with a finite element Maxwell equations solver Amaze 3D (Field Precision, Albuquerque, NM). In case of multiple nsEP exposures, the interval between stimuli was 0.5 or 1 sec.

Results and Discussion

We reported earlier that nsEP permeabialized plasma membrane similarly in GH3, Jurkat, and PC12 cells[13]. In this study, we compared the effect in GH3 cells, which express multiple types of endogenous ion channels [14] and CHO-K1 cells, which express very few channels [15]. In both cell lines, nsEP caused a characteristic long-lasting increase of the whole-cell conductance with profound rectification of the inward current. Although the extent of rectification varied, it was observed in most if not all nsEP-treated cells.

Three different examples of inward rectification are presented in Fig. 1. Panel (**a**) compares current-voltage (I–V) characteristics in cells subjected to 0 (control), 2.4, or 4.8 kV/cm nsEP. The recording pipette was kept away from the cells until after the nsEP, to prevent any potential artifacts from the pipette presence when the pulse is applied. However, with this experiment protocol, the I–V data could only be collected with a 100–140 sec post-nsEP delay needed to establish the whole-cell configuration. Despite this delay, nsEP-treated cells displayed profound enhancement of inward current, but no change or even inhibition of the outward current.

Next, we found that the presence of the recording pipette does not alter nsEP effects (at least at low pulse amplitudes), and that the inward rectification is not caused by different ion composition of the bath buffer and the cytoplasm. To prove it, the pipette and bath solutions were made identical, and the whole-cell configuration was established 2–3 min prior to nsEP application, to allow enough time for dialysis of the cytoplasm with the pipette buffer. The symmetrical solution conditions did not eliminate the inward rectification: nsEP increased the

inward current, but had little or no effect on the outward one (Fig. 1b, c and Fig. 2). For a cell shown in Fig. 1b, it took about a minute for the pores to reseal, and the whole-cell conductance restored fully to its pre-exposure level. In many other cells, however, this was not the case; instead, the outward current at a positive membrane potential increased abruptly, followed by the loss of rectification and propidium uptake (Fig. 1c and Fig 2). This transition is best explained by a breakdown of nanopores into larger, propidium-permeable, non-rectifying "conventional" pores. The breakdown occurred always at positive membrane potentials, which, together with the inward rectification, suggested functional and structural asymmetry of nsEP-opened pores.

The resting membrane potential of living cells adds to the externally applied E-field at the anodic pole of the cell and attenuates it at the cathodic pole. As a result, external EPs porate cells preferentially from the anodic pole, where the inside of the membrane is charged negatively [1,16]. To test if this E-field direction at the site of pore formation is the cause of nanopore asymmetry, we cancelled the resting membrane potential by clamping it at 0 mV prior to nsEP application, making the probability of pore formation at either pole of the cell approximately equal. As an example, the cell shown in Fig. 2 was held at 0 mV membrane potential when exposed to nsEP, and was permeabilized from the cathodic pole. Now, nanopores were formed at the pole where the membrane was positive inside, but it did not change the nanopores' properties: they still displayed inward rectification and broke into the propidium-permeable, non-rectifying pores at positive membrane potentials. This finding proved that it was not the transmembrane E-field direction, but the intrinsic asymmetry of the cell membrane that caused the functional asymmetry of nanopores.

The formation of nanopores and their extended lifetime were independently verified by non-electrophysiological methods, namely by fluorescent detection of cell uptake of small inorganic cations. The best results were achieved by loading cells with a Tl^+-sensitive fluorophore and using Tl^+ uptake as a marker for nanoporation (Fig 3). An obvious advantage of using Tl^+-dependent fluorescence as compared to common Na^+, K^+, or Ca^{2+} detection techniques is that Tl^+ is not present in living cells in any considerable amount; hence, even very small amounts of Tl^+ entering from the outside can be detected. To prevent potential Tl^+ entry through voltage-gated K^+ channels (in an unlikely case if these channels are activated by nsEP and remain open for minutes), the bath buffer contained high concentrations of several K^+ channel antagonists. An immediate, dose-dependent surge in Tl^+ uptake was readily detected in either GH3 or CHO cells exposed to nsEP in a Tl^+-containing buffer (Fig 3a). Note that Tl^+ uptake was triggered at the E-field intensities far below the threshold for propidium uptake.

Alternatively, cells could be stimulated by nsEP in a solution that contained isoosmotic quantity of Cs^+ instead of Tl^+, so that no immediate change in cell fluorescence occurred. The time course of resealing of nanopores was probed by the addition of the Tl^+-containing bath buffer at various intervals after nsEP. The experiments established that nsEP-treated cells remain highly permeable to Tl^+ even 5–10 min after the nsEP (Fig 3b). This result supports earlier findings using patch-clamp [13] that the lifetime of nsEP-opened nanopores is on the order of minutes.

The formation of lipid nanopores is a logical extension of the well-established conventional electroporation phenomenon, and a smaller size of nsEP-opened pores has been predicted by modeling [10,11]. Further evidence that nsEP-opened nanopores are not protein ion channels comes from observations of fast externalization of PS residues. In healthy undisturbed cells, PS residues are found only or mostly on the internal face of the cell membrane; they can "flip" to the outside by either enzymatic action in the course of apoptosis, or by drifting out along the surface of a lipid pore (see Vernier et al., 2004 for detailed discussion). On the contrary, the pore of protein-made ion channels lacks the continuity of the lipid-water interface from the

inside to the outside face of the membrane, and therefore does not provide the passageway for PS translocation. NsEP caused PS externalization within just seconds (much faster than in the course of apoptosis) and often without propidium uptake (Fig. 4a). A more intense nsEP treatment resulted just in borderline propidium staining (Fig. 4b). Under the same recording conditions, chemical poration of the membrane with digitonin caused immense propidium entry and saturation of the fluorescence detector within seconds (Fig. 4c). Of note, formation of nanopores by nsEP led to cell swelling and blebbing (Fig. 4, DIC images), but forming larger, propidium-permeable pores with digitonin had an opposite effect of implosion of blebs.

Overall, both the theoretical models and experimental findings provided matching evidence for lipid nanopore opening by nsEP, but did not explain how these nanopores are able to exert complex conductive behaviors that are thought to be a prerogative of highly specialized, protein-made ion channels. An answer may unexpectedly come from recent studies in synthetic nanopores that were engineered in a polymer foil by heavy particle bombardment and subsequent etching from one side [17]. Resulting conically-shaped nanopores had I–V characteristics remarkably similar to those seen in our study: they passed ion currents preferentially in one direction, changed conductance in response to applied voltage, showed ion selectivity and single channel-like conductance fluctuations. These and other properties of synthetic nanopores have been detailed in later publications [18–20] and appear at least partially applicable to nsEP-opened nanopores in live cells. The asymmetrical, conical shape can in principle explain complex properties of nanopores in live cells, but it has yet to be demonstrated how such a shape can actually be maintained.

In our study, nsEP stimulation was a convenient and efficient method to produce nanopores “on demand” to analyze their properties; however, there is no reason to believe that this is the only or unique way to open nanopores. In fact, it is not unusual to see nanopore-like electric currents without any electrostimulation, but they cannot be reliably differentiated from the gigaohmic seal deterioration in a standard patch-clamp experiment. Hence, when such currents are observed, they often receive little attention and are discarded as an artifact or a sign of cell rundown. However, here we showed that nanopores are not an artifact; they can be detected by both electrophysiological and fluorescent methods, and do not depend on the presence of the recording pipette. We demonstrated that nanopores are long-lasting membrane formations which can significantly affect transmembrane ion flows and are adequately equipped for certain functions that are traditionally ascribed to classic ion channels. For instance, unidentified non-specific cation channels have been implicated in many physiological processes, e.g., cell swelling and blebbing after exposure to ROS donors [21], after oxygen-glucose deprivation [22], and following ATP depletion [23]. Nanopore formation could reasonably be an additional (if not an alternative) mechanism of these changes, but this possibility has not been considered by investigators who traditionally focused on protein ion channels; many more similar examples can be found. Clear distinction between nanopores-conducted and ion channels-conducted currents may be critical for understanding how these currents are activated and controlled in physiological and pathological conditions.

Acknowledgements

We thank Dr. V. Gabai (Boston University Medical School, Boston, MS) for discussions and help with data interpretation and Dr. S. Xiao (Old Dominion University, Norfolk, VA) for designing the nanosecond pulse source and calculating E-field distribution. The work was supported by R01CA125482 from the National Cancer Institute.

References

1. Neumann, E.; Sowers, AE.; Jordan, CA., editors. Electroporation and Electrofusion in Cell Biology. New York: Plenum; 1989.

2. Teissie J, Golzio M, Rols MP. Mechanisms of cell membrane electropermeabilization: a minireview of our present (lack of ?) knowledge. Biochim Biophys Acta 2005;1724:270–280. [PubMed: 15951114]
3. Heller LC, Heller R. In vivo electroporation for gene therapy. Hum Gene Ther 2006;17:890–897. [PubMed: 16972757]
4. Sersa G, Miklavcic D, Cemazar M, Rudolf Z, Pucihar G, Snoj M. Electrochemotherapy in treatment of tumours. Eur J Surg Oncol 2008;34:232–240. [PubMed: 17614247]
5. Pakhomov AG, Shevin R, White JA, Kolb JF, Pakhomova ON, Joshi RP, Schoenbach KH. Membrane permeabilization and cell damage by ultrashort electric field shocks. Arch Biochem Biophys 2007;465:109–118. [PubMed: 17555703]
6. Beebe SJ, Fox PM, Rec LJ, Willis EL, Schoenbach KH. Nanosecond, high-intensity pulsed electric fields induce apoptosis in human cells. Faseb J 2003;17:1493–1495. [PubMed: 12824299]
7. Vernier PT, Sun Y, Marcu L, Salem S, Craft CM, Gundersen MA. Calcium bursts induced by nanosecond electric pulses. Biochemical and Biophysical Research Communications 2003;310:286–295. [PubMed: 14521908]
8. Pakhomov AG, Phinney A, Ashmore J, Walker K, J K, Kono S, Schoenbach KS, Murphy MR. Characterization of the cytotoxic effect of high-intensity, 10-ns duration electrical pulses. IEEE Transactions on Plasma Science 2004;32:1579–1585.
9. Vernier PT, Sun Y, Marcu L, Craft CM, Gundersen MA. Nanoelectropulse-induced phosphatidylserine translocation. Biophys J 2004;86:4040–4048. [PubMed: 15189899]
10. Gowrishankar TR, Weaver JC. Electrical behavior and pore accumulation in a multicellular model for conventional and supra-electroporation. Biochem Biophys Res Commun 2006;349:643–653. [PubMed: 16959217]
11. Smith KC, Weaver JC. Active mechanisms are needed to describe cell responses to submicrosecond, megavolt-per-meter pulses: cell models for ultrashort pulses. Biophys J 2008;95:1547–1563. [PubMed: 18408042]
12. Vernier PT, Sun Y, Gundersen MA. Nanoelectropulse-driven membrane perturbation and small molecule permeabilization. BMC Cell Biol 2006;7:37. [PubMed: 17052354]
13. Pakhomov AG, Kolb JF, White JA, Joshi RP, Xiao S, Schoenbach KH. Long-lasting plasma membrane permeabilization in mammalian cells by nanosecond pulsed electric field (nsPEF). Bioelectromagnetics 2007;28:655–663. [PubMed: 17654532]
14. Stojilkovic SS, Zemkova H, Van Goor F. Biophysical basis of pituitary cell type-specific Ca2+ signaling-secretion coupling. Trends Endocrinol Metab 2005;16:152–159. [PubMed: 15860411]
15. Maroto R, Raso A, Wood TG, Kurosky A, Martinac B, Hamill OP. TRPC1 forms the stretch-activated cation channel in vertebrate cells. Nat Cell Biol 2005;7:179–185. [PubMed: 15665854]
16. Weaver JC. Electroporation of cells and tissues. IEEE Trans. Plasma Sci 2000;28:24–33.
17. Siwy Z, Gu Y, Spohr HA, Baur D, Wolf-Reber A, Spohr R, Apel P, Korchev YE. Rectification and voltage gating of ion currents in a nanofabricated pore. Europhys. Lett 2002;60:349–355.
18. Cervera J, Schiedt B, Neumann R, Mafe S, Ramirez P. Ionic conduction, rectification, and selectivity in single conical nanopores. J Chem Phys 2006;124:104706. [PubMed: 16542096]
19. Ramirez P, Gomez V, Cervera J, Schiedt B, Mafe S. Ion transport and selectivity in nanopores with spatially inhomogeneous fixed charge distributions. J Chem Phys 2007;126:194703. [PubMed: 17523824]
20. Kosinska ID. How the asymmetry of internal potential influences the shape of I–V characteristic of nanochannels. J Chem Phys 2006;124:244707. [PubMed: 16821996]
21. Barros LF, Hermosilla T, Castro J. Necrotic volume increase and the early physiology of necrosis. Comp Biochem Physiol A Mol Integr Physiol 2001;130:401–409. [PubMed: 11913453]
22. Lipski J, Park TIH, Li D, Lee SCW, Trevarton AJ, Chung KKH, Freestone PS, Bai J-Z. Involvement of TRP-like channels in the acute ischemic response of hippocampal CA1 neurons in brain slices. Brain Research 2006;1077:187–199. [PubMed: 16483552]
23. Gabai VL, Kabakov AE, Mosin AF. Association of blebbing with assembly of cytoskeletal proteins in ATP-depleted EL-4 ascites tumour cells. Tissue Cell 1992;24:171–177. [PubMed: 1589868]

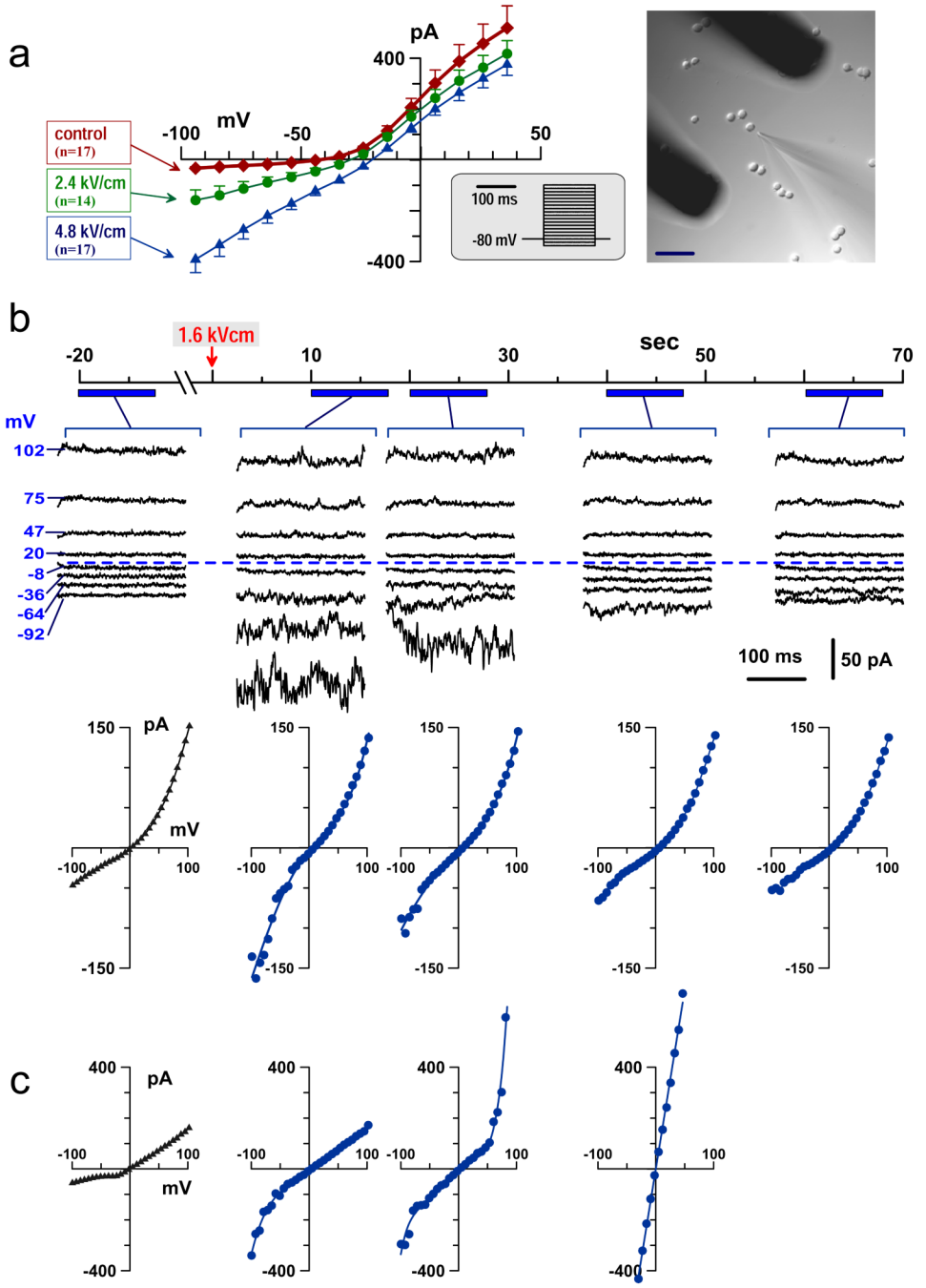

Fig. 1.

Inward rectification of the whole-cell current in nsEP-treated GH3 cells. (a) Effect of nsEP applied to intact cells (before attaching the recording pipette). Currents were measured in 100–140 sec after nsEP. Shown are mean values ± SE for *n* independent, randomized experiments. Insets show the voltage step protocol and the position of nsEP-delivering electrodes relative to the exposed cell and the recording pipette. Calibration bar: 50 μm. (b, c) Effect of nsEP under symmetrical solution conditions; cells were dialyzed with pipette solution prior to nsEP. The timeline applies to both (b) and (c); nsEP was applied at 0 sec (arrow). Currents were repeatedly probed by a voltage step protocol during intervals indicated under the timeline. Shown are both the original current traces and corresponding current-voltage (I–V) plots (b),

or I–V-plots only (c). Dashed line identifies zero current. Nanopores either gradually resealed (b), or broke into highly conductive, non-rectifying pores (c).

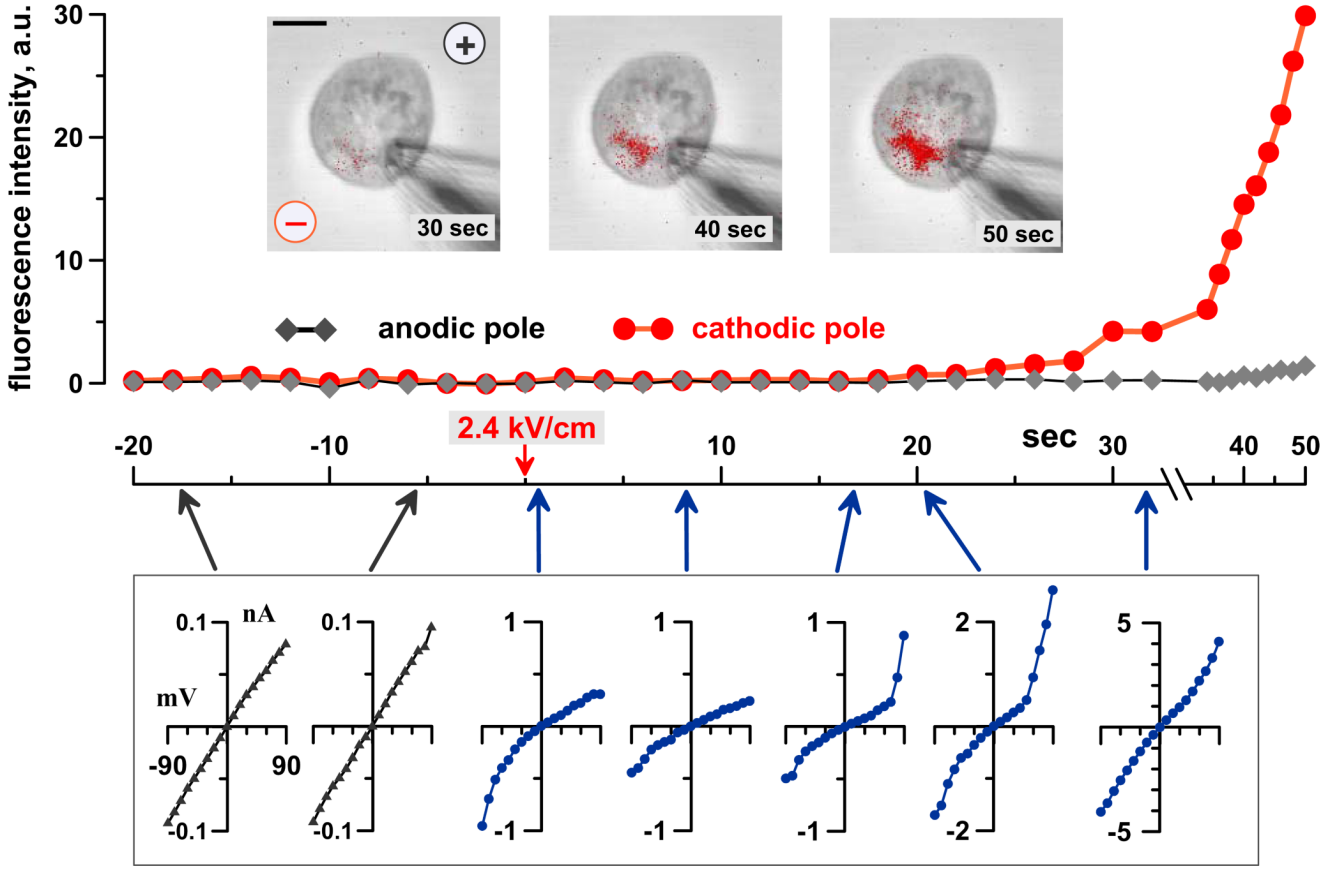

Fig. 2.

Localized propidium uptake marks transformation of nsEP-opened nanopores into more conductive, non-rectifying larger pores. Images of a GH3 cell were taken and whole-cell currents were probed every 2 sec. The bath and pipette solutions were identical, except for addition of 30 μg/ml PI to the bath. The cell was held at 0 mV membrane potential when stimulated by nsEP at 0 sec. Propidium emission was measured separately at the anodic and cathodic poles of the cell. Insets: propidium fluorescence (red) laid over DIC images of the cell (grey) at indicated time intervals after nsEP. “Plus” and “minus” symbols identify the position and polarity of nsEP-delivering electrodes. Calibration bar: 5 μm. Plotted below the graph are characteristic I–V data recorded at the time points identified by arrows; note different vertical scales. NsEP increased membrane currents, with profound inward rectification, but did not induce any propidium uptake. After a brief recovery, currents abruptly increased at a positive membrane potential, immediately followed by a localized propidium uptake and the loss of inward rectification.

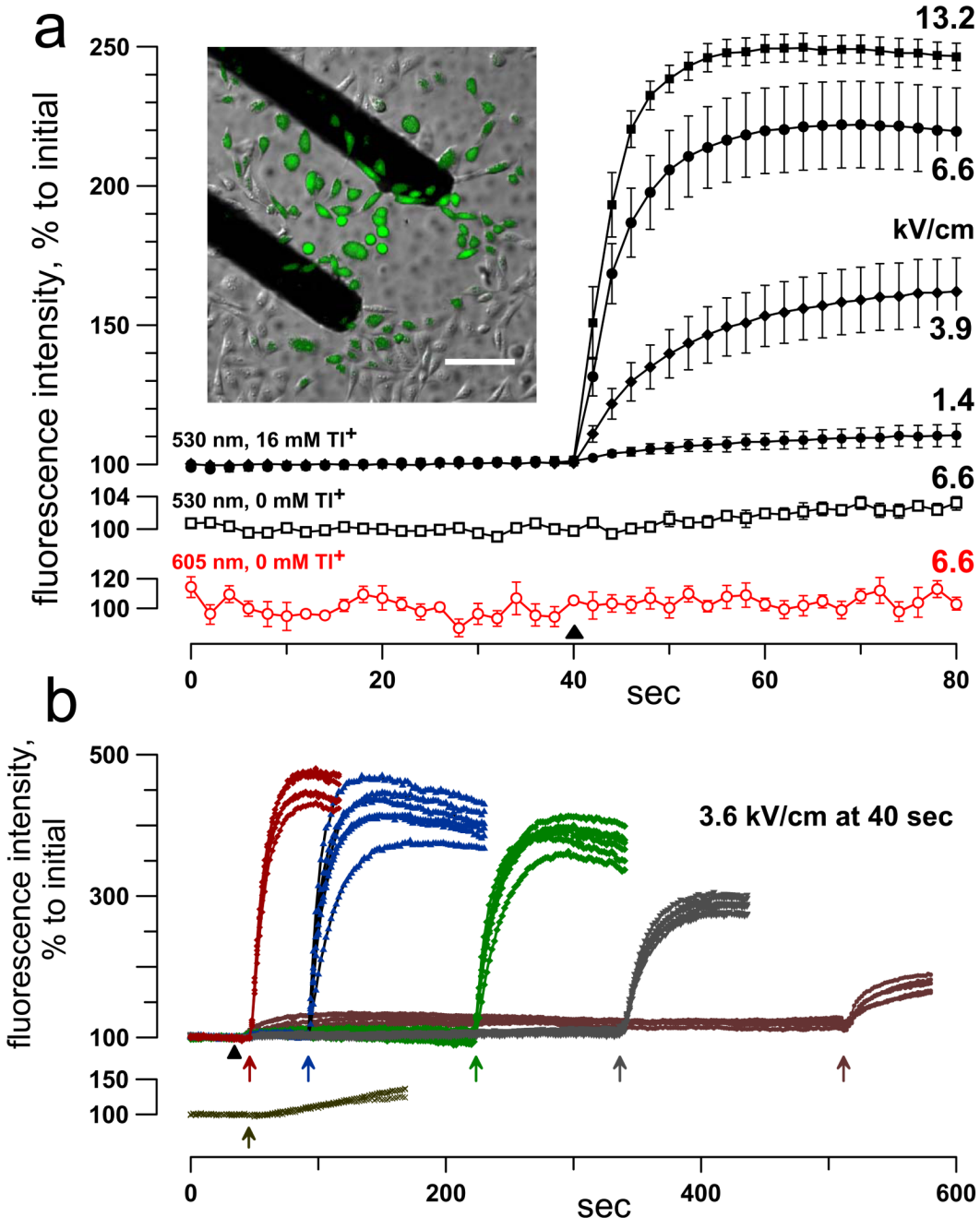

Fig. 3.

Nanopore detection by fluorescence imaging of Tl^+ uptake. (a) NsEP triggers a dose-dependent uptake of Tl^+, but cells remain impermeable to propidium. CHO cells were pre-loaded with FluxOR dye and bathed in a solution with either 16 mM Tl^+ (filled symbols; top graphs) or 0 mM Tl^+ (open symbols); the solutions also contained 30 μg/ml PI. Images were taken every 2 sec using 530 and 605 nm bandpass filters for Tl^+ and propidium emission signals, respectively. NsEP of indicated intensity (kV/cm) was applied at 40 sec (black triangle). NsEP profoundly enhanced emission at 530 nm (when Tl^+ was present) and had no effect on 605 nm emission. Shown are mean values ± SE for 6 to 12 cells per group. The inset shows selective Tl^+ uptake by nsEP-exposed cells between nsEP-delivering electrodes, 20 sec after one 8.8

kV/cm pulse. Calibration bar: 100 μm. (b): The lifespan of nanopores was probed by delayed application of a Tl^+-containing bath buffer. Upper graphs: FluxOR-loaded CHO cells were stimulated with a 3.6 kV/cm pulse at 40 sec (filled triangle) in a solution that contained no Tl^+. Addition of a Tl^+-containing buffer at various time intervals after nsEP (arrows) caused immediate surge of Tl^+ uptake. In contrast, same change of buffers caused just a weak, gradual response in cells that were not stimulated by nsEP (lower graph).

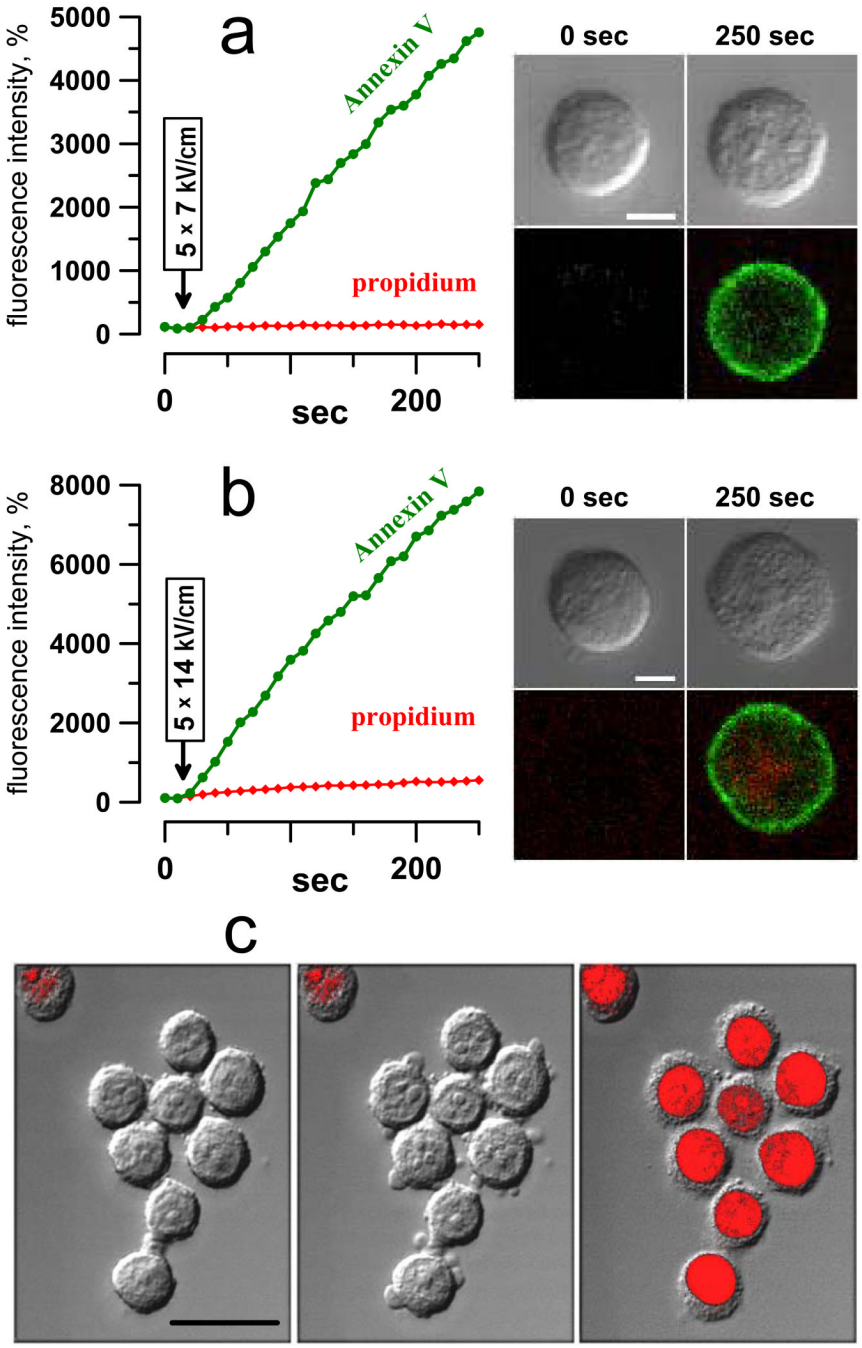

Fig. 4.

Formation of nanopores leads to phosphatidylserine externalization, cell swelling and blebbing. (a, b): Changes in Annexin V-FITC and propidium fluorescence in GH3 cells caused by a train of 5 nsEP at 7 kV/cm (a) or 14 kV/cm (b); the onset of the train is indicated by arrows. Right panels show respective DIC images (top) and superimposed Annexin V-FITC (green) and propidium (red) fluorescence at the bottom. Note immediate PS externalization without propidium uptake (a) or with minimum uptake after a more intense nsEP treatment (b). Also note swelling of nsEP-treated cells. (c) Blebbing in GH3 cells subjected to a train of 40 pulses at 4.4 kV/cm. All three panels show propidium fluorescence (red) on top of DIC images. One cell, in the top left corner, was propidium-positive already before the treatment. From left to

right: immediately prior to nsEP, 1 min after it, and 10 sec after permeabilization of cells by 0.1% digitonin. Note that digitonin also caused implosion of blebs. Calibration bars: 5 μm (a, b) and 20 μm (c).